TA 8f.

FORSCHUNG - AUSBILDUNG - WEITERBILDUNG

Bericht Nr. 41

MULTISCALE ANALYSIS, WAVELETS AND TEXTURE QUALITY

Hans-Georg Stark

UNIVERSITÄT KAISERSLAUTERN
Fachbereich Mathematik
Erwin-Schrödinger-Straße
D - 6750 Kaiserslautern

Januar 1990

MULTISCALE ANALYSIS, WAVELETS AND TEXTURE QUALITY

Hans-Georg Stark
Fachbereich Mathematik, Universität Kaiserslautern
D-6750 Kaiserslautern, F.R.G.

Abstract

Fleeces made from artificial fabric are the basic material for many products, ranging from carpets to napkins. It turns out that their quality is determined by the distribution of the fibres, which can be measured either by the optical transmission properties or by the thickness of the material. In both cases one obtains a 2-dimensional signal and one would like to have an objective quality criterion, based on a suitable analysis of these data, which, moreover, can be automated.

In this paper we propose a solution to this problem, based on multiresolution techniques, which have been developed in image analysis through the last few years. Moreover we use these techniques to investigate fractal properties of the textures.

Index Terms - Image Analysis, Quality Control, Multiresolution Techniques, Wavelet Transformation, Fractals

I. Introduction

In this paper we address the problem of asserting quality attributes to certain kinds of textures which are produced in industrial processes. To be specific, consider a fleece, made from artificial fabric, like in fig. 1. Here and in all following images of this type we use digitized pictures consisting of 512×512 pixels, whose intensities are coded by one out of 256 possible colour levels with blue corresponding to 0 and yellow corresponding to 255. Thus our data may be described by a matrix c^{o}_{ik} (i=1,...,512; k=1,...,512) with integer entries between 0 and 255 (the meaning of the upper case index "o" will be clear below). Fleeces of this type are the basic material of many products, ranging from napkins to carpets. Clearly discriminable are essentially two features, namely

- clouds, consisting of large clusters of adjacent fibres, having no preferred direction, and
- stripes of some adjacent fibres sticking together and showing a preferred direction.

It turns out that these factors are essential for the quality of the fleece in the following sense: Large clouds deteriorate the optical appearance of the material, since they don't look pleasing. Stripes deteriorate the mechanical properties, since a large number of stripes, all having about the same direction, can give rise to some anisotropy of the material with respect to tensile strength. Up to now the quality of the fleece, i.e. the influence of the above-mentioned factors, was simply estimated by some experienced persons and a majority decision was made, which clearly has some disadvantages. Therefore a quantitative quality measure is desired, which moreover can be used for automatic monitoring of the production process, since through a

long term production run usually the fleece quality deteriorates.

Thus the problem may be formulated as follows: Find a suitable set of numbers, measuring the contribution of stripes, the contribution of clouds and anisotropy. To formulate it alternatively: Find a suitable concept of distance of the given pattern to the ideal uniform (i.e. all c^o_{ik} are equal) one, which is sensitive to stripes, clouds, anisotropy.

In order to illustrate the basic concepts we shall focus on one-dimensional cuts (i.e. data of the form c^o_i (i=1,...,N)), thus disregarding the problem of anisotropy for a while. It turns out that the method we propose has an immediate generalization to two dimensions and anisotropy may be treated easily.

In one dimension "clouds" simply correspond to large scale features with low spatial frequency and "stripes" to small scale features, whose spatial frequency is relatively large. One of the most simple ideas to measure the irregularity of the given signal would be to compute the square of the ℓ_2-distance of the given signal to the uniform distribution i.e. essentially the square of the variance of the signal: With

$$\langle c^o \rangle = \frac{1}{N} \sum_{i=1}^{N} c^o_i$$

compute

$$\sum_{i=1}^{N} (c^o_i - \langle c^o \rangle)^2 \sim \sigma^2 .$$

But this measure cannot distinguish between clouds and stripes: The "cloud" of fig. 2 gives the same value as the set of "stripes".

The same reasoning applies to any quality measure of the type

$\sum_{i=1}^{N} f(c_i^o)$, since for the computation of the sum the order of the numbers in the sequence $\{c_i^o\}_{i=1}^N$ is irrelevant. Thus any quality concept based on ℓ_p-distances or entropy is excluded. For a measure theoretic alternative to these distance concepts, which does not suffer from the above mentioned drawbacks, we refer to [1]. The point of view we want to adopt is the following: Clouds and stripes are treated as scale phenomena with clouds corresponding to large scale features and stripes corresponding to small scale features. Now try to construct a sequence of signals in which a priori information about scales is implemented, as indicated below. Since we have a priori information about scales, we are free, then, to use ℓ_p-concepts again on these scaled versions. Thus we want to associate to the given signal c^o a sequence of signals d^a, labelled by a scale parameter a (>0) and indicating the presence of structures of typical size a as illustrated in fig. 3.

In order to treat anisotropy it would also be advantageous to have direction sensitive devices of this type. Moreover on line requirements necessitate fast algorithms for the computation of such signals.

Fortunately such scaling algorithms exist in image analysis.We mention explicitly the Laplacian Pyramid of Burt and Adelson [2] and the conjugate quadrature filters (CQF) of Smith and Barnwell [3]. In this paper we use a decomposition technique developed by S. Mallat [4] using the theory of wavelet transformation [5], which turns out to be closely related to CQF's and can be very easily applied to two dimensions. For a compact formulation of Mallat's algorithm see [6], the relation to CQF's is explored in more detail also in [7].

We turn now to a short description of the organization of the paper: Section II contains a review of Mallat's wavelet-based decomposition scheme [4] essentially as presented in [6].
In section III we first describe the generalization to the 2-d-case. Then the proposed quality numbers are motivated and introduced. This procedure is tested by the discussion of several examples.
In the last section we study fractal properties of these textures since it turns out that multiscale methods are well adapted for that purpose. This gives an interesting link to the work of Pentland [8], [9], who uses a fractal model for the description of natural scenes.

II. Wavelets and Multiscale Methods

We present here Mallat's multiresolution algorithm [4] essentially as described in [6].
Let us first recall some basic notions of square integrable functions. The space $L^2(\mathbb{R})$ consists of all complex valued functions f on the real line such that

$$\int |f(x)|^2 dx < \infty \ . \tag{1}$$

On this space an inner product is defined by

$$(f,g) := \int \overline{f}(x)g(x)dx \ , \tag{2}$$

which associates to each $f \in L^2(\mathbb{R})$ its norm $\|f\|$ by

$$\|f\|^2 = (f,f) \ . \tag{3}$$

A complete orthonormal basis (ONB) consists of a countable set of functions ψ_k ($k \in \mathbb{Z}$) with

$$(\psi_i, \psi_k) = \begin{cases} 1 & \text{if } i=k \\ 0 & \text{else} \end{cases} \ , \tag{4}$$

such that each $f \in L^2(\mathbb{R})$ may be expanded uniquely as

$$f = \sum_i (\psi_i, f)\psi_i \quad . \tag{5}$$

The same notations and definitions also apply to closed linear subspaces of $L^2(\mathbb{R})$. We have mentioned these facts mainly in order to fix the notation. Some familiarity of the reader with these concepts is assumed and for more detailed information we refer to standard texts like [10].

A "dyadic multiscale analysis" is a sequence $\{V_j\}_{j\in\mathbb{Z}}$ of closed subspaces $V_j \subset L^2(\mathbb{R})$ having the following properties:

1. The sequence is monotonic, i.e. $\ldots \subset V_{j+1} \subset V_j \subset V_{j-1} \subset \ldots$

2. $V_j \xrightarrow{j\to\infty} \{0\}$, $V_j \xrightarrow{j\to-\infty} L^2(\mathbb{R})$

3. $f(x) \in V_j$ if and only if $f(2x) \in V_{j-1}$

4. There exists some $\phi \in V_o$ such that the set of functions $\phi(x-k)$ $(k \in \mathbb{Z})$ constitutes an ONB of V_o. ϕ is called "scaling function".

One concludes easily that all the spaces V_j are built from V_o simply by rescaling: $f(x) \in V_j$ if and only if $f(2^j x) \in V_o$. Moreover from 3 and 4 follows that $2^{-j/2}\phi(2^{-j}x-k)$ defines an ONB of V_j, if k varies over $\mathbb{Z}$.

One can choose [11] ϕ such that the spaces V_j consist of functions which are piecewise polynomial on intervals $[k\cdot 2^j,(k+1)2^j)$ $(k \in \mathbb{Z})$. Thus the projection of f onto V_j corresponds to the construction of a "sketchy" [11] version of f in which on each of the above intervals f is approximated by a polynomial function. In this way by projecting f onto V_j details of size smaller than 2^j are suppressed (but, of course, in a way which

depends on ϕ) and by projecting onto V_{j-1} one obtains the "next better" approximation.

It is now interesting to look at the increase of information going from the projection onto V_j to the projection onto V_{j-1} and therefore one studies the orthogonal complement W_j of V_j with respect to V_{j-1} fulfilling

$$V_j \oplus W_j = V_{j-1} \quad . \tag{6}$$

One can show [7] that there exists a function $\psi \in W_o$ satisfying a certain "admissibility criterion" [5], a socalled "wavelet", such that $2^{-j/2}\psi(x\cdot 2^{-j}-k)$ defines an ONB of W_j, if k varies over $\mathbb{Z}$. Thus with

$$\psi_{jk}(x) := 2^{-j/2}\psi(2^{-j}x-k) \tag{7}$$

and ϕ_{jk} analogously defined the set $\{\phi_{jk}\}_{k\in\mathbb{Z}}$ defines an ONB of V_j and $\{\psi_{jk}\}_{k\in\mathbb{Z}}$ defines an ONB of W_j. For convenience let us denote from now on with $c^j(f)$ the projection of $f \in L^2(\mathbb{R})$ onto V_j and with $d^j(f)$ the projection onto W_j.

We already note that the W_j spaces should be interesting for our purpose: If $f \in L^2(\mathbb{R})$ represents our signal, $d^j(f)$ measures the <u>difference</u> of two successive approximations, i.e. projections $c^j(f)$ and $c^{j-1}(f)$, respectively. Thus, if in our original signal structures of a typical size between 2^j and 2^{j-1} are present, they should be localized by $d^j(f)$ as indicated in fig. 3.

Let our sampled signal be given by a sequence $\{c_i^o\}$ such that $\sum_i (c_i^o)^2 < \infty$ as mentioned in the introduction. Then it is imbedded into V_o by defining

$$f(x) := \sum_i c_i^o \phi(x-i) \tag{8}$$

(i.e.: the sampling distance corresponds to 1). Let us define

the sequences c_i^j and d_i^j via projecting f onto V_j and W_j, respectively, and expanding with respect to the corresponding basis systems:

$$c^j(f) = \sum_i c_i^j \, \phi_{ji} \tag{9}$$

and

$$d^j(f) = \sum_i d_i^j \, \psi_{ji} \ . \tag{10}$$

Thus the calculation of $c^j(f)$ is equivalent to calculating the sequence $\left\{c_i^j\right\}$ and analogously for $d^j(f)$ and $\left\{d_i^j\right\}$. Now an easy calculation shows that

$$c_i^j = \sum_k h(k-2i) c_k^{j-1}$$

and (11)

$$d_i^j = \sum_k g(k-2i) c_k^{j-1}$$

with

$$h(m) = (\phi_{1o}, \phi_{om})$$

and (12)

$$g(m) = (\psi_{1o}, \phi_{om}) \ .$$

Defining on ℓ_2 (the space of square summable sequences) the filters H and G by $(\{z_i\} \in \ell_2$, i.e.: $\sum_i |z_i|^2 < \infty)$

$$(Hz)_i := \sum_k h(k-2i) z_k$$

and (13)

$$(Gz)_i := \sum_k g(k-2i) z_k \ ,$$

respectively, the wavelet decomposition takes the simple hierarchical form as indicated in fig. 4. Note the occurrence of the factor 2 in formula (13), which results in decimating our

sequences: In each step their length is divided by 2.
One can check [6], [7] that H and G satisfy certain conditions which Barnwell and Smith [3] impose on their "conjugate quadrature filters" (CQF), which they use for their signal decomposition and reconstruction scheme. Thus wavelet filters belong to the class of CQF's, but they additionally fulfill a certain regularity condition [7], which turns out to be very useful for applications in signal analysis.

III. Proposed Quality Numbers and Discussion of Examples

As described in the preceding section, a wavelet decomposition (like any multiscale analysis, based on CQF's) results in a decomposition of the original signal $\{c_i^o\} \equiv c^o$ into a sequence $c^J, d^J, d^{J-1}, \ldots, d^1$ of signals, where the integer $J \geq 0$ indicates the coarsest scale level 2^J up to which (starting from 1) the decomposition is made. d^j $(j=1,\ldots,J)$ indicates the contribution of scale factors between 2^{j-1} and 2^j.
Starting from images (2-d-signals) $\{c_{ik}^o\}$ one can use filter pairs H^cH^r, H^cG^r, G^cH^r with, for example, H^c denoting the H-filter from (13) but acting only on the column index of a two dimensional signal. Analogously H^r acts only on the row index and the same conventions apply to G^c and G^r. With these filter pairs the two-dimensional signal $c^o \equiv \{c_{ik}^o\}$ is decomposed now into a sequence $\{c_{ik}^J\} \equiv c^J, d^{Jh}, d^{Jv}, d^{(J-1)h}, d^{(J-1)v}, \ldots, d^{1h}, d^{1v}$ (see [4]), where the signal $\{d_{ik}^{jv}\} \equiv d^{jv}$ indicates the presence of <u>vertical</u> structures "living on" scales between 2^{j-1} and 2^j and analogously for d^{jh} and <u>horizontal</u> structures. This decomposition also has a simple hierarchical structure analogously to that for one dimension, indicated in fig. 4 [4]. One can also define indicators for diagonal structures, but we don't use them

here. Thus in the 2-d-case in addition to the scale label j (j=1,...,J) our d-signals also obtain a direction label (h or v) for two orthogonal directions which makes them useful for judging anisotropy properties of the material as described below. In this context it is promising for future activities that one might be able to choose wavelets with "tunable" directions [12].

Before introducing our evaluation scheme we note as an aside that if we have a quadratic picture of area ℓ^2 (with ℓ denoting the side length of the image), digitized by 512×512 pixels, then obviously a scale factor 2^j corresponds to a typical size of $(\frac{\ell}{512})2^j$ (since now the sampling distance is $\frac{\ell}{512}$ instead of 1), thus, in our decompositions above, stage j corresponds to typical sizes between $(\frac{\ell}{512})2^{j-1}$ and $(\frac{\ell}{512})2^j$ (in vertical or horizontal direction, respectively).

Let 2^{2N} denote the total number of pixels in the original image (in the examples discussed here we have $2^N=512$). We take then the decimating effect, expressed by the factor 2 in formula (11) into account (i.e. the number of pixels in the d^j-images is reduced at each step by 2×2=4) and define the average intensity value of the signal d^{jv} as

$$\langle d^{jv} \rangle = 2^{-2(N-j)} \sum_{i,k} |d^{jv}_{ik}| \qquad (14)$$

(analogously for $\langle d^{jh} \rangle$). The square of the variance is defined as

$$(\sigma^{jv})^2 = 2^{-2(N-j)} \sum_{i,k} (|d^{jv}_{ik}| - \langle d^{jv} \rangle)^2 \qquad (15)$$

(analogously for $(\sigma^{jh})^2$).

Now, since we consider the d^j-signals to be "scale indicators"

in the sense of section I (fig. 3) in which a-priori-information about scales is implemented, we shall use the ℓ_2-concept again and propose the following procedure:

1. Choose some integer $J>0$ and decompose the image $c^o \equiv \{c^o_{ik}\}$ according to $c^J, d^{Jh}, d^{Jv}, d^{(J-1)h}, d^{(J-1)v}, \ldots, d^{1h}, d^{1v}$.
2. Calculate the variances $(\sigma^{jh})^2$ (analogously $(\sigma^{jv})^2$), indicating the presence of horizontal (vertical) structures of typical size between $\left(\frac{\ell}{2^N}\right)2^{j-1}$ and $\left(\frac{\ell}{2^N}\right)2^j$ $(j=1,\ldots,J)$.
3. As a measure for anisotropy (on each scale level) calculate the quotients

$$a_j := \frac{(\sigma^{jv})^2}{(\sigma^{jh})^2} \qquad (j=1,\ldots,J) \; . \tag{16}$$

Thus stripes should be characterized by high variance-values on relatively small j-levels and corresponding anisotropy values, which are remarkably different from 1, whereas on the other hand clouds should correspond to high variance values on large j-levels and corresponding anisotropy values, which do not differ too much from 1.

In the examples discussed below we have $2^{2N} = 512\times512$ and $J=5$, thus the sizes, which are indicated by the decomposition should roughly lie in between $\frac{\ell}{512}$ and $\frac{\ell}{16}$. Moreover, in order to get comparable results, we chose a normalization such that the maximum of $|d^{jx}_{ik}|$ $(j=1,\ldots,J;x=v,h;(i,k)$ varies over all pixels of $d^{jx})$ corresponds to a given, fixed value (in our case 255).

The first example, we discuss, is shown in fig. 5. Looking at this fleece one has the impression that stripes of a certain intermediate thickness are oriented preferably along the vertical axis. This feeling is clearly confirmed by the anisotropy

plot, shown in fig. 5a, where the anisotropy numbers a_j, defined by equation (16), are plotted vs. j. This plot shows a pronounced maximum with value 3.34 at j=3. As explained above this means a strong vertical dominance for structures with typical size between $\frac{\ell}{128}$ and $\frac{\ell}{64}$, i.e. the presence of - essentially vertically oriented - stripes of thickness roughly between $\frac{\ell}{128}$ and $\frac{\ell}{64}$. We also learn from this plot that there is a horizontal dominance for j=1 (a_1=0.18). This means that very thin (single) fibres of the material are essentially horizontally directed, which is not so easily deduced simply by visual inspection, but it also can be confirmed. Of course a simple explanation of the horizontal dominance at j=1 would be that the more vertically oriented single fibres are covered by gross structures which are essentially vertically oriented.

As explained in the preceding section one can use wavelets which are piecewise polynomial, and it is to be expected that filters based on smoother wavelets (i.e. with higher polynomial degree) extract more accurately the characteristic features of the signal itself, i.e. with less disturbance caused by the wavelet, than filters based on wavelets with lower polynomial degree. This is illustrated in fig. 5b, where the anisotropy plot of fig. 5a which was based on piecewise linear wavelets is compared with the corresponding plot for piecewise quadratic wavelets. As expected the characteristics of the fleece are more pronounced with quadratic wavelets, where the extrema in the anisotropy values are even better separated than in the linear case.

To illustrate the scale dependence of the anisotropy plots consider fig. 6, where, due to an error in the data, there is a thin, only a few pixels wide, vertical strip, which is reflected

by the corresponding anisotropy plot (fig. 6a), where the maximum of vertical dominance is shifted towards lower scale values, as compared to fig. 5a. The maximum value (a_2=2.85) is not as large as the maximum value (a_3=3.34) of fig. 5a corresponding to the fact that the anisotropy of example 2 is caused by one single stripe only.

As a last example for anisotropy consider fig. 7. Here the horizontal dominance at the smallest scale level (single fibres) is more easily seen than in fig. 5 which results in an a_1-value (0.077) which is lower than the coresponding value (0.093) of example 1 (see fig. 7a, where the anisotropy plot of example 3 is drawn). Fig. 7a tells also that, as expected, the maximum of example 3 at j=3 is less than a_3 of example 1, where the visual impression of vertical anisotropy is larger than in example 3. It is interesting that the dark horizontal boundary zones of example 3 lead to a remarkable horizontal dominance at the coarsest scale level 5 with anisotropy number clearly below 1, since the corresponding size $\frac{\ell}{16}$ is now in the order of the width of these boundary regions.

Thus there is experimental evidence that the anisotropy numbers a_j (j=1,...,J) are a good quantitative measure for the degree of anisotropy in the corresponding scale levels, thus giving useful information about the distribution of the material. We note as an aside that, as expected, the anisotropy values tend towards 1 for large scale levels ("clouds" have no preferred direction.

Finally we check the significance of the magnitude of the numbers $(\sigma^{jv})^2$ and $(\sigma^{jh})^2$, respectively. Comparing example 4 (fig. 1) with example 2 (fig. 6), we see that (possibly due to

illumination conditions) the image of fig. 1 has much more contrast than the image of fig. 6. Putting it alternatively this means that in example 4 at each stage of resolution much more structure is present than in example 2 and this is reflected in fig. 8, where the quotient $(\sigma^{jh})^2_{ex.\ 4} / (\sigma^{jh})^2_{ex.2}$ is plotted vs. j. This quotient is at all stages much larger than 1.

Comparing example 3 (fig. 7) with example 5 (fig. 9) at first sight we see no large difference. However careful inspection shows that example 5 is slightly more blurred than example 3. Of course this blurring will mainly affect the fine details; fig. 7 should show more structure, especially on small scale levels, than fig. 9. This is exactly the case in fig. 10, where $(\sigma^{jh})^2_{ex.3} / (\sigma^{jh})^2_{ex.5}$ is plotted vs. j. This quotient is always greater than 1, due to this blurring effect, but obviously the blurring affects mainly the small scale levels, the scale dominance of example 3 decreases, as j, and therefore the resolved detail size, increases.

Thus the set of 3J numbers $(\sigma^{jv})^2$, $(\sigma^{jh})^2$, a_j (j=1,...,J), obtained by a decomposition obviously might be useful as an objective criterion for texture quality, i.e. measuring scale contributions and anisotropy.

IV. Fractal Properties

Since the following treatment applies to vertical as well as horizontal directions, we shall omit the direction index in the formulae below.

The presentation of the data discussed in this section is motivated by the fact that it is not really satisfying, to check the dominance of certain scales with respect to reference fleeces,

as done in fig. 8, and one would like to have criteria, which are independent from e.g. illumination conditions such as the intensity of the incoming light. To this end we want to employ the spatial correlations of the $|d^j_{ik}|$-pixel values.
Choose with some fixed numbers $\beta>0$ and $\alpha\geq 0$

$$\gamma_j = \beta \, \langle d^j \rangle^{-1} 2^{j\alpha} \, . \tag{17}$$

Now renormalize the signal by defining

$$\tilde{d}^j_{ik} = \gamma_j d^j_{ik} \, . \tag{18}$$

Then, with $(\tilde{\sigma}^j)^2$ denoting the square of the variance of the renormalized signal, clearly

$$(\tilde{\sigma}^j)^2 = \gamma_j^2 (\sigma^j)^2 = \beta^2 2^{2j\alpha} \frac{(\sigma^j)^2}{\langle d^j \rangle^2} \tag{19}$$

and the total intensity of the renormalized signal reads (note again the decimating effect!)

$$\begin{aligned} \tilde{I}_j = \sum_{i,k} |\tilde{d}^j_{ik}| = \langle \tilde{d}^j \rangle 2^{2(N-j)} &= \gamma_j \langle d^j \rangle 2^{2(N-j)} \\ &= \beta \, 2^{2N} \, 2^{-j(2-\alpha)} \end{aligned} \tag{20}$$

We shall say that our fleece has "uniform scale behaviour" if its $|d^j_{ik}|$ values basically obey the same statistics for all $j=1,\ldots,J$, thus, particularly

$$\frac{(\sigma^{j+1})^2}{\langle d^{j+1} \rangle^2} \approx \frac{(\sigma^j)^2}{\langle d^j \rangle^2} \qquad j=1,\ldots,J-1 \, . \tag{21}$$

An immediate consequence is that for fleeces showing uniform scale behaviour

$$\frac{(\tilde{\sigma}^{j+1})^2}{(\tilde{\sigma}^j)^2} \approx 2^{2\alpha} \, , \tag{22}$$

therefore a semilog plot of $(\tilde{\sigma}^j)^2$ vs. j should roughly be a straight line with slope given by (22). We remark that, if we obtain some "maximal" decorrelation of neighboring pixels in the

d^j-images, i.e. if there are no strong spatial correlations in the d^j-images, then it is plausible that the $|d^j_{ik}|$-values will be approximately Poisson-distributed, in which case

$$\frac{(\sigma^{j+1})^2}{\langle d^{j+1}\rangle^2} = \frac{(\sigma^j)^2}{\langle d^j\rangle^2} = 1 \ . \qquad (23)$$

The idea is now that dominant scales are characterized by a significant deviation from uniform scale behaviour, i.e. when plotting $(\tilde{\sigma}^j)^2$ semilogarithmically vs. j at the corresponding scale levels there should be deviation from the straight line law.

This is illustrated in fig. 11 and fig. 12, where $(\tilde{\sigma}^{jh})^2$ of example 1 and $(\tilde{\sigma}^{jv})^2$ of example 2 are plotted semilogarithmically vs. j. The thin vertical strip of example 2 leads to a deviation from the straight line law at j=1, whereas it is fulfilled very well for $(\tilde{\sigma}^{jh})^2$ of example 1. In both figures we chose α=2, i.e. (cf. formula (20)) the d^j-images were renormalized to a fixed intensity.

We note that in all fleeces checked so far the "uniform scale behaviour" seems to be well fulfilled with a value of the quotient $\frac{(\sigma^{j+1})^2}{\langle d^{j+1}\rangle^2} \Big/ \frac{(\sigma^j)^2}{\langle d^j\rangle^2}$ varying roughly between 0.9 and 1 (as long as no scale dominance in the above sense is noted). Moreover (with this same restriction) the value of $\frac{(\sigma^j)^2}{\langle d^j\rangle^2}$ for all j and all fleeces is about 0.7,...,0.8, which is not so far from Poisson distribution, where this factor should be 1. Since this value is essentially independent from the particular fleece, (19) implies that the straight line obtained by plotting $(\tilde{\sigma}^j)^2$ semilogarithmically vs. j should be roughly the same for all fleeces. This is illustrated in figures 13a and 13b, where the semilog plots of $(\tilde{\sigma}^{jh})^2_{ex.4}$ and $(\tilde{\sigma}^{jh})^2_{ex.1}$ and of $(\tilde{\sigma}^{jh})^2_{ex.2}$ and $(\tilde{\sigma}^{jh})^2_{ex.4}$, respectively, are plotted in one diagram. Here again

we chose $\alpha=2$. Still some more detailed statistical analysis of the data (fit and test of distribution laws) should be carried out.

The concept of uniform scale behaviour discussed here bears some relation to selfsimilarity, a basic principle in the description of fractals [13], and we shall shortly discuss a possible connection to fractals. Pentland [8], [9] has proposed a description of natural scenes, based on a certain fractal model, namely Brownian noise. For a detailed discussion of fractals we refer to [13] and [8]. We only mention here that in the case of images Brownian noise may be characterized by some scale factor α with $0<\alpha<1$ and its fractal dimension, which is correlated to the psychophysical perception of roughness [8] and reads $D=3-\alpha$. Mallat [4] has shown that, if one performs a wavelet decomposition of a realization of Brownian fractal noise with scale factor α, one obtains precisely the law (22). Thus, putting these observations together, we see that, provided our fleeces show uniform scale behaviour, by renormalizing them corresponding to (17), (18) with $0<\alpha<1$, we can convert them at least to behave fractal like in the sense of (22). Moreover, this provides a correlation between roughness and intensities of scale contributions, which makes sense: Since $D=3-\alpha$ measures roughness [8] and by (20) the intensities $\tilde{I}_j$ of the $\tilde{d}^j$-images obey $\tilde{I}_j \sim 2^{-(2-\alpha)j}$, we see that large roughness (α small) corresponds to a fast decrease of $\tilde{I}_j$ with increasing j, i.e. for rough textures small scales (j small) show relatively high intensities as compared to large scales (large j) and vice versa for "smooth textures" and large α.

Thus, provided one performs a renormalization, the fractal model for natural textures also might be useful for "man made

textures" like the fleeces discussed here, as long as they show uniform scale behaviour, which of course is related to their production process.

Acknowledgement

I am indebted to Q. Chen, who implemented Mallat's multiresolution scheme on the computer and to J. Struckmeier for providing me with a graphics facility.

References

[1] B. Wetton and H. Neunzert, Pattern Recognition using Measure Space Metrics, Rep. No. 28 of AGTM, Kaiserslautern, 1987

[2] P. Burt and E. Adelson, The Laplacian Pyramid as a Compact Image Code, IEEE Trans. on Communications, Vol. Com-31, No. 4, pp. 532-540, April 1983

[3] M. Smith and T. Barnwell, Exact Reconstruction Techniques for Tree-Structured Subband Coders, IEEE Trans. on Acoust., Speech and Signal Processing, Vol. ASSP-34, No. 3, pp. 434-441, June 1986

[4] S. Mallat, A Theory for Multiresolution Signal Decomposition: The Wavelet Representation, Dept. of Computer and Information Science, University of Pennsylvania, preprint, May 1987

[5] J.M. Combes, A. Grossmann and Ph. Tchamitchian (eds.), Wavelets, Springer-Verlag, Berlin, Heidelberg, New York, 1989

[6] I. Daubechies, Orthonormal Bases of Wavelets with Finite Support-Connection with Discrete Filters, in: Wavelets, J.M. Combes, A. Grossmann and Ph. Tchamitchian (eds.), Springer-Verlag, Berlin, Heidelberg, New York, 1989

[7] I. Daubechies, Orthonormal Bases of Compactly Supported Wavelets, Comm. Pure and Appl. Math., Vol. 49, pp. 909-996, 1988

[8] A. Pentland, Fractal-Based Description of Natural Scenes, IEEE Trans. on Pattern Analysis and Machine Intelligence, Vol. PAMI-6, No. 6, November 1984

[9] A. Pentland, Fractal-Based Description of Natural Scenes, in: Proc. IEEE Conf. Comput. Vision and Pattern Recognition '83, Arlington, VA, July 1983

[10] M. Reed and B. Simon, Methods of Modern Mathematical Physics I: Functional Analysis, 2nd ed., Academic Press, New York, 1980

[11] Y. Meyer, Orthonormal Wavelets, in: Wavelets, J.M. Combes, A. Grossmann and Ph. Tchamitchian (eds.), Springer-Verlag, Berlin, Heidelberg, New York, 1989

[12] R. Murenzi, Wavelet-Transforms Associated to the n-Dimensional Euclidean Group with Dilations: Signals in More than One Dimension, in: Wavelets, J.M. Combes, A. Grossmann and Ph. Tchamitchian (eds.), Springer-Verlag, Berlin, Heidelberg, New York, 1989

[13] B.B. Mandelbrot, Die Fraktale Geometrie der Natur, Birkhäuser-Verlag, Basel, Boston, 1987

Figure Captions

Fig. 1 Example 4

Fig. 2 Clouds and Stripes

Fig. 3 Original Signal c^0 and Scale Indicators

Fig. 4 Wavelet Decomposition

Fig. 5 Example 1

Fig. 5a Anisotropy of Example 1

Fig. 5b Anisotropy of Example 1 with linear (Solid Line) and Quadratic (Broken Line) Wavelets

Fig. 6 Example 2

Fig. 6a Anisotropy of Example 2

Fig. 7 Example 3

Fig. 7a Anisotropy of Example 3

Fig. 8 $(\sigma^{jh})^2_{ex.4} \,/\, (\sigma^{jh})^2_{ex.2}$ vs. j

Fig. 9 Example 5

Fig. 10 $(\sigma^{jh})^2_{ex.3} \,/\, (\sigma^{jh})^2_{ex.5}$ vs. j

Fig. 11 Semilog Plot of $(\tilde{\sigma}^{jh})^2_{ex.1}$ vs. j

Fig. 12 Semilog Plot of $(\tilde{\sigma}^{jv})^2_{ex.2}$ vs. j

Fig. 13a Semilog Plot of $(\tilde{\sigma}^{jh})^2_{ex.4}$ (Solid Line) and $(\tilde{\sigma}^{jh})^2_{ex.1}$ (Broken Line) vs. j

Fig. 13b Semilog Plot of $(\tilde{\sigma}^{jh})^2_{ex.4}$ (Solid Line) and $(\tilde{\sigma}^{jh})^2_{ex.2}$ (Broken Line) vs. j

Footnotes

The author is with Fachbereich Mathematik, Universität Kaiserlautern, Postfach 3049, D-6750 Kaiserslautern, F.R.G.

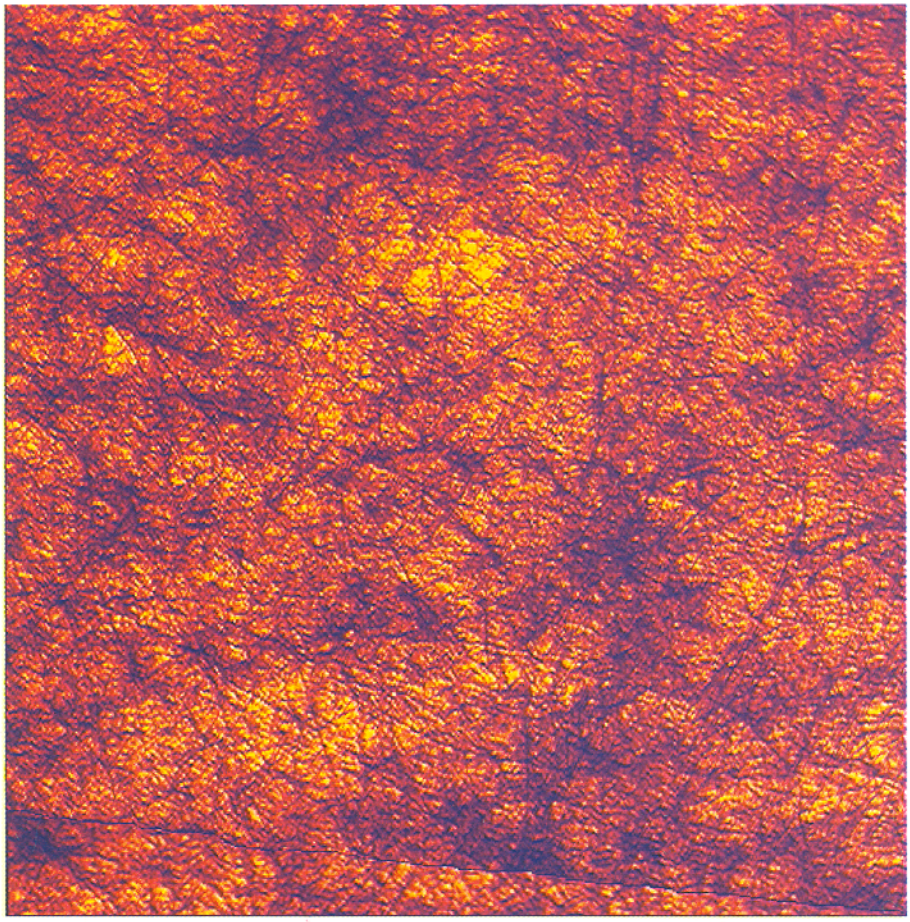

↑ horizontal direction

⟶ vertical direction

Fig. 1: Example 4

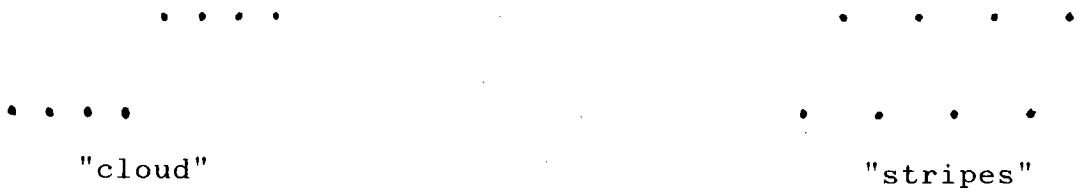

Fig. 2: Clouds and stripes

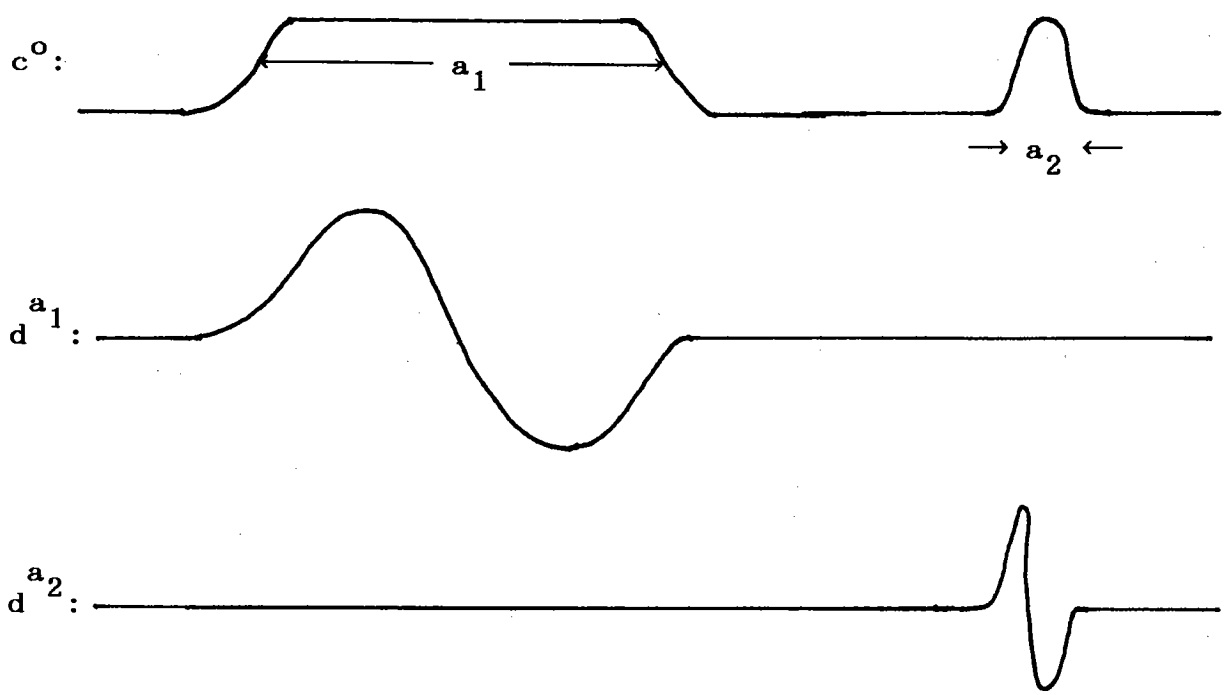

Fig. 3: Original signal c^o and scale indicators

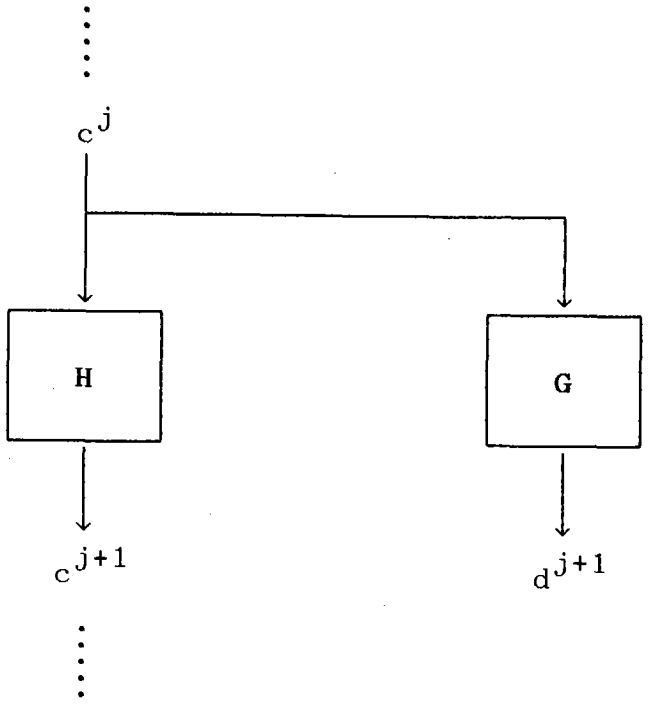

Fig. 4: Wavelet decomposition

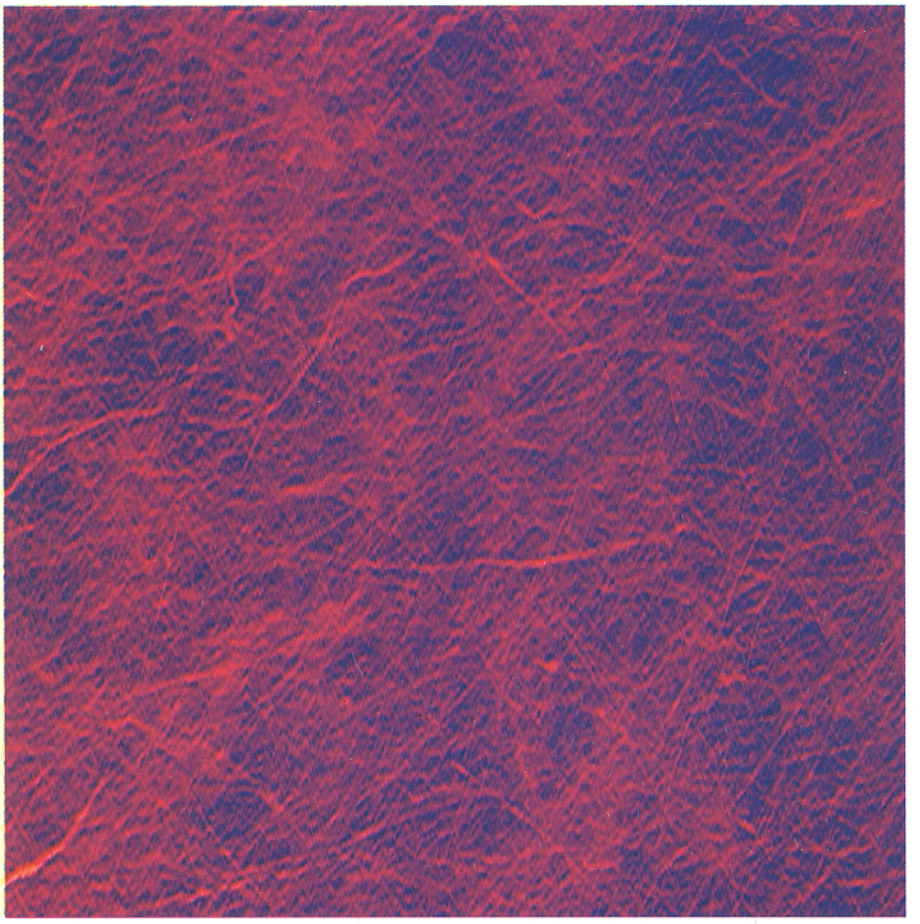

Fig. 5: Example 1

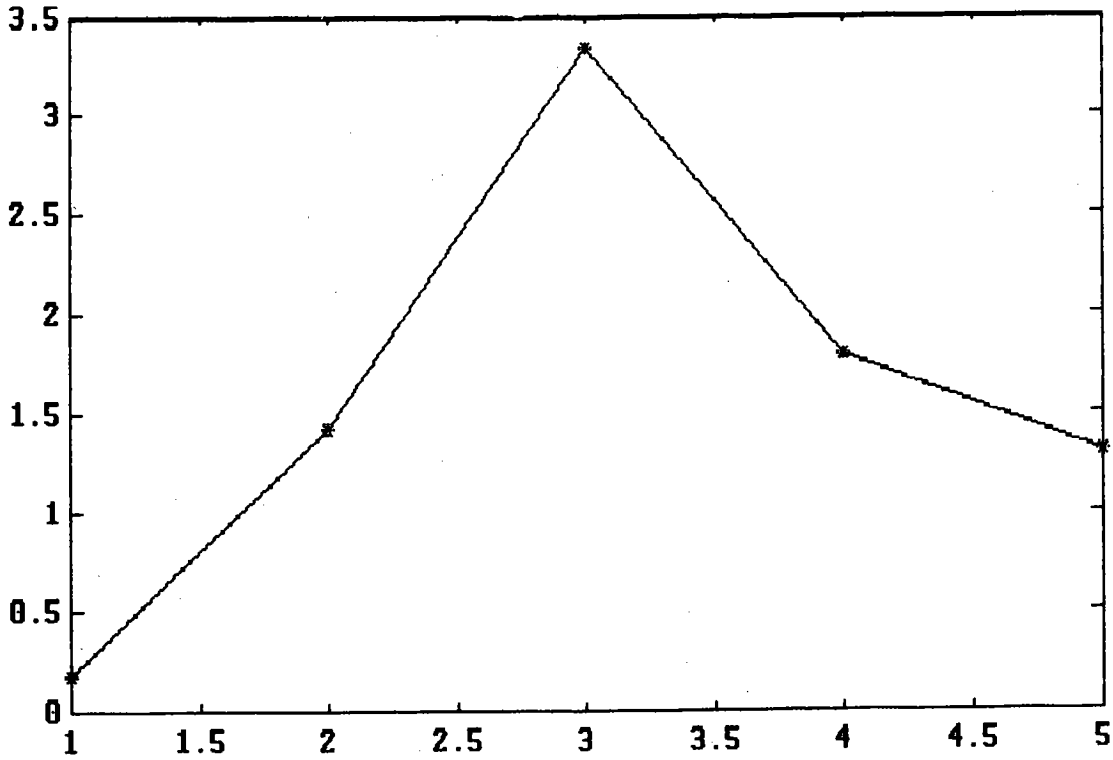

Fig. 5a: Anisotropy of example 1

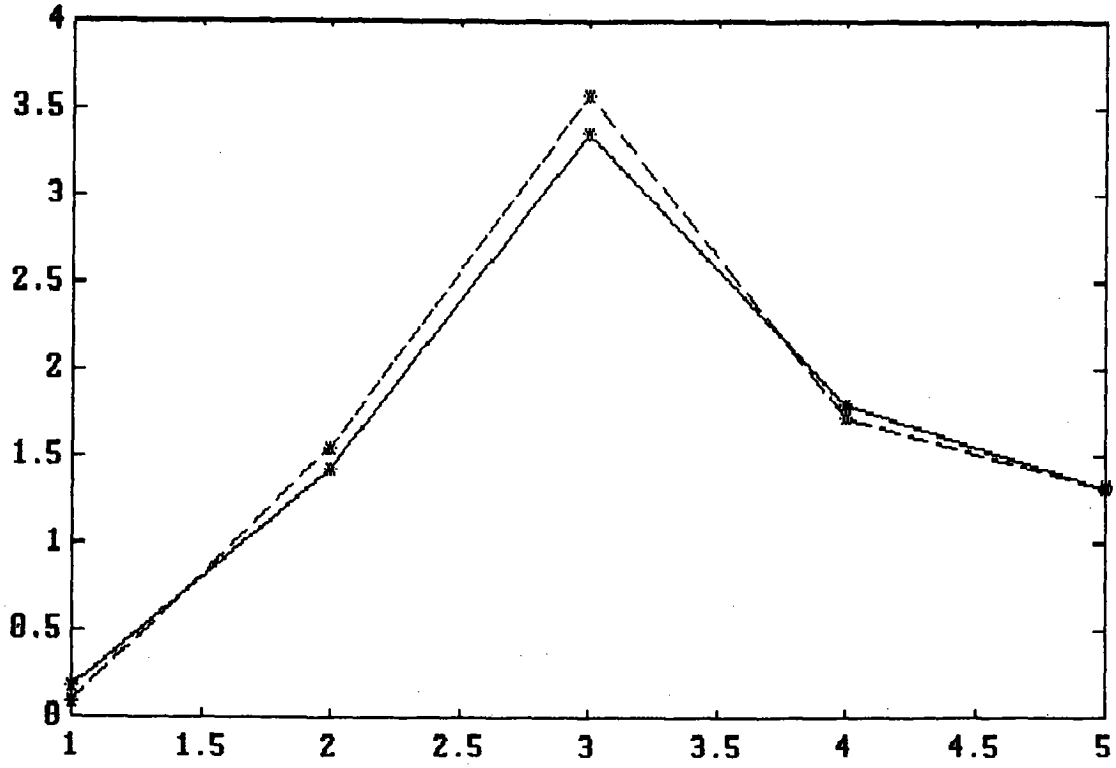

Fig. 5b: Anisotropy of example 1 with linear (solid line) and quadratic (broken line) wavelets

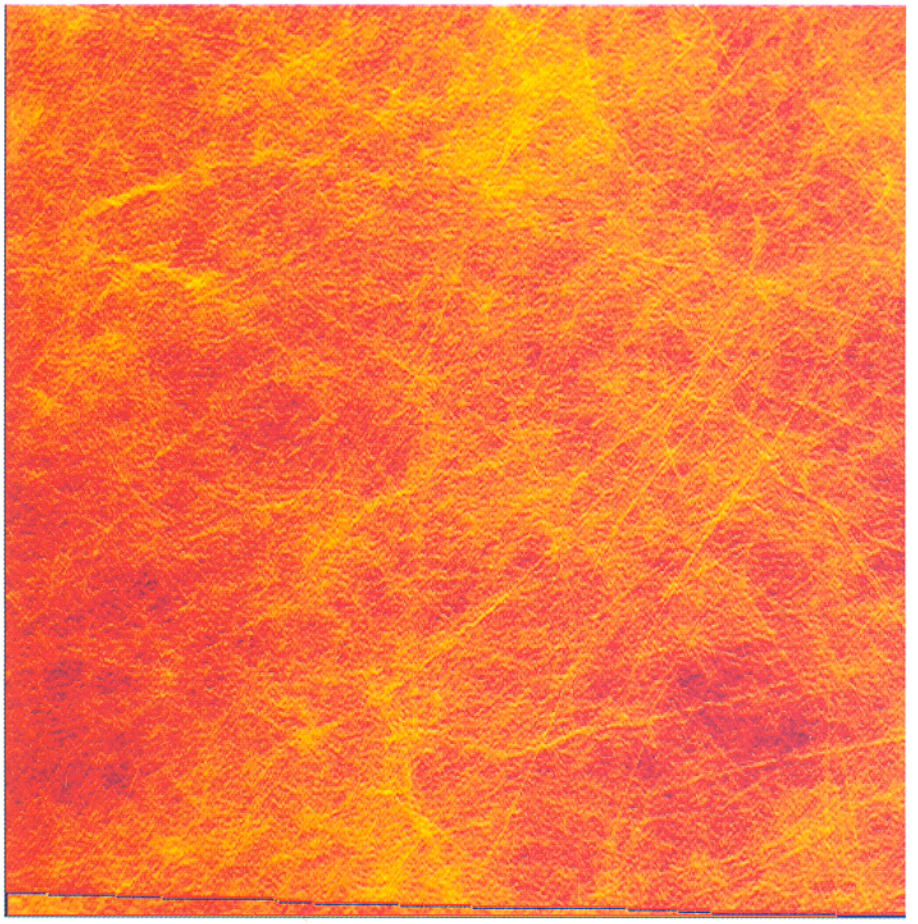

Fig. 6: Example 2

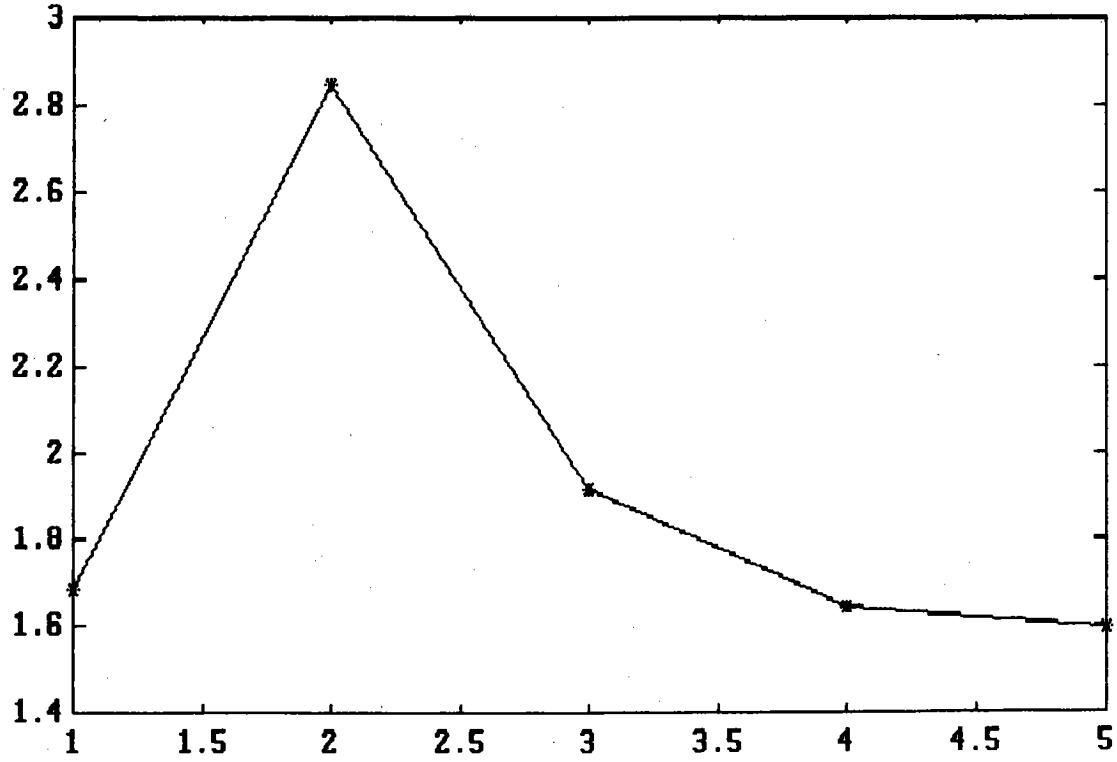

Fig. 6a: Anisotropy of example 2

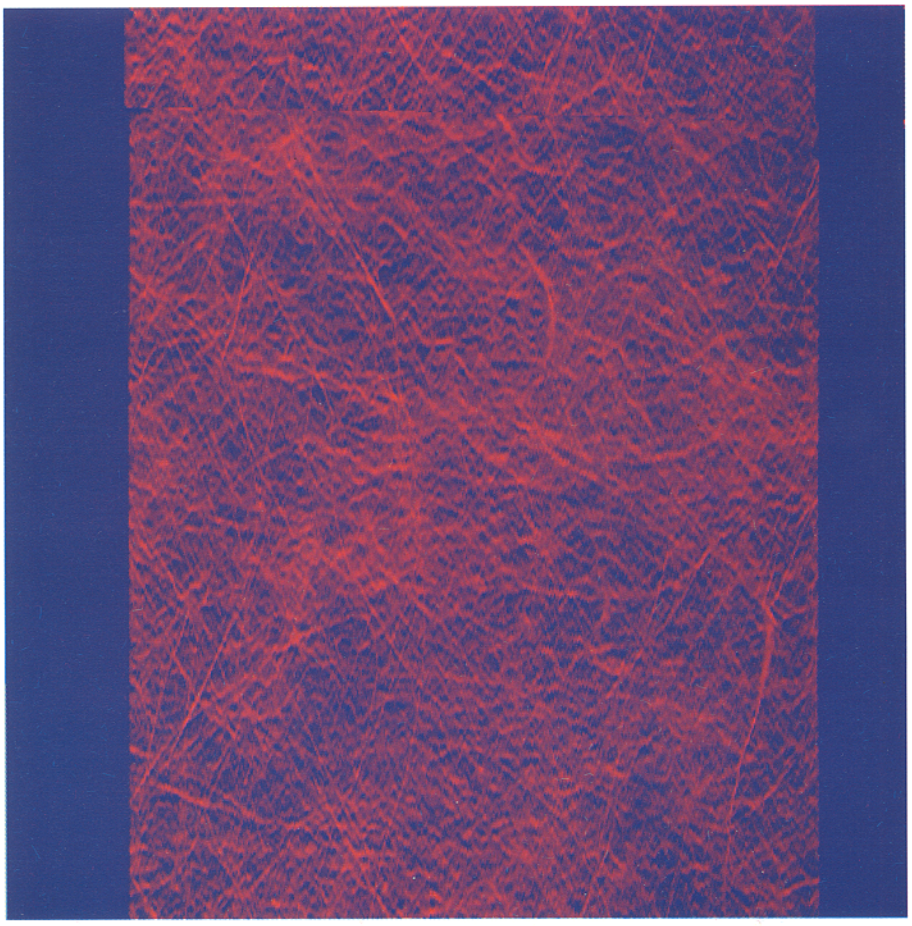

Fig. 7: Example 3

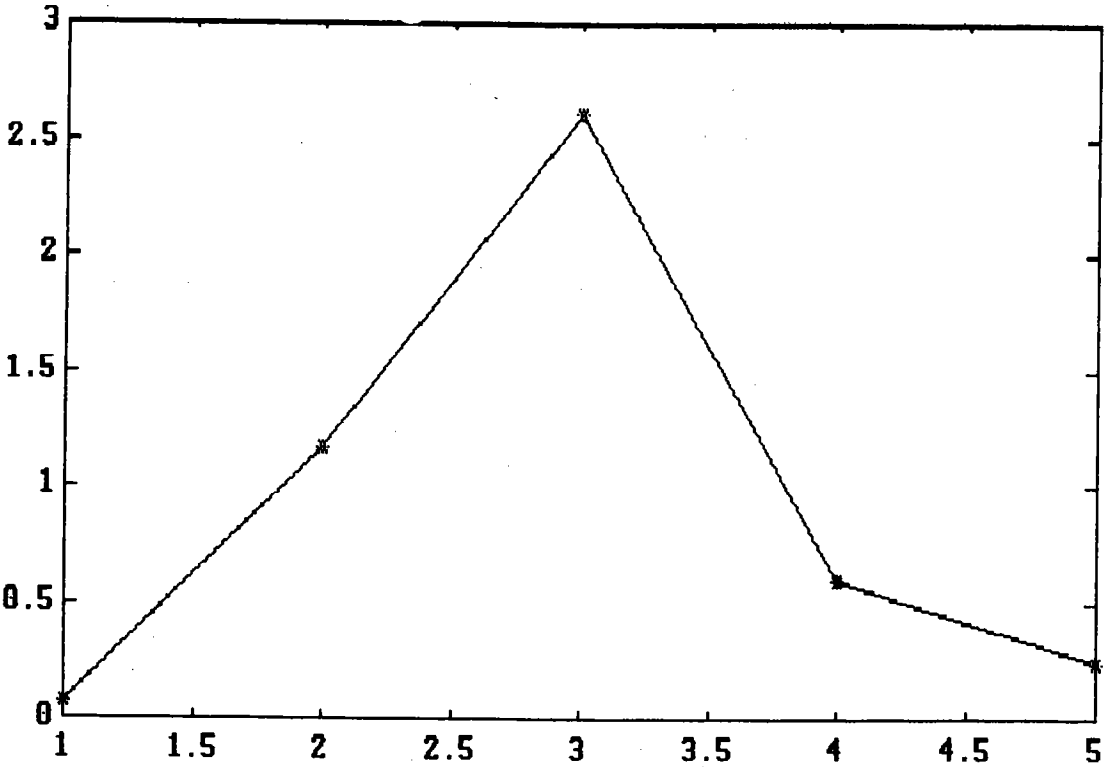

Fig. 7a: Anisotropy of example 3

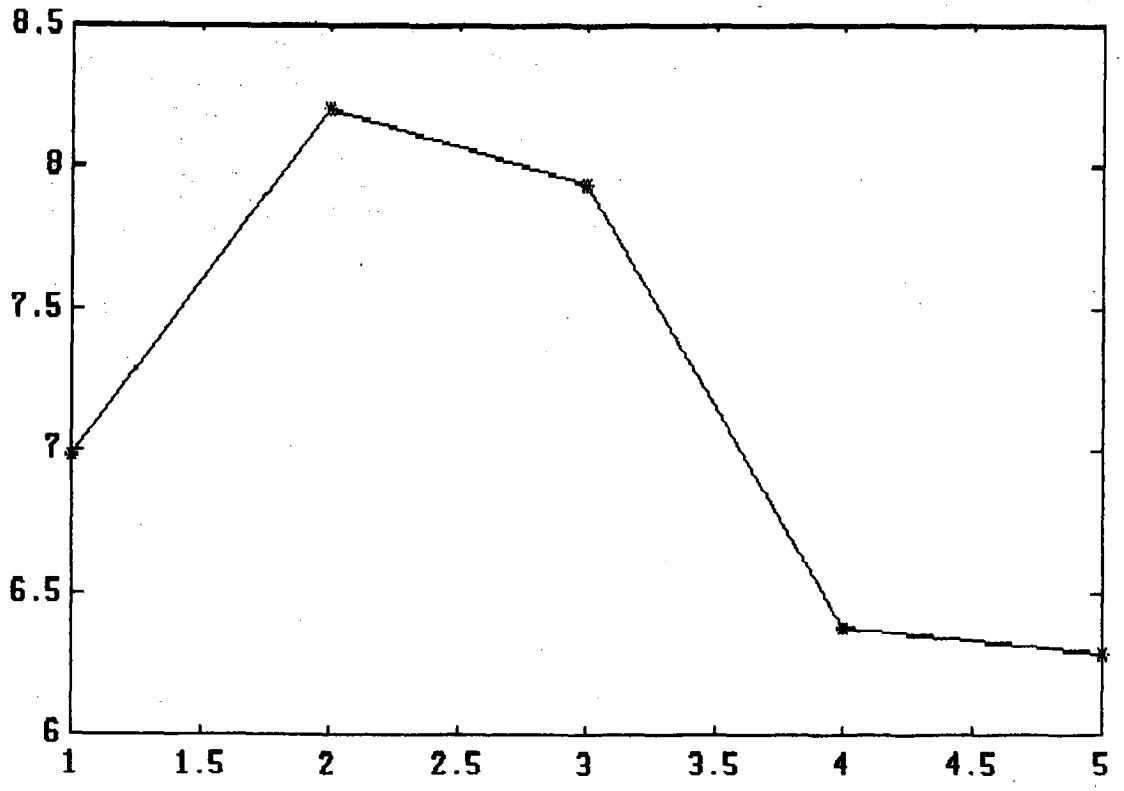

Fig. 8: $(\sigma^{jh})^2_{ex.4}$ / $(\sigma^{jh})^2_{ex.2}$ vs. j

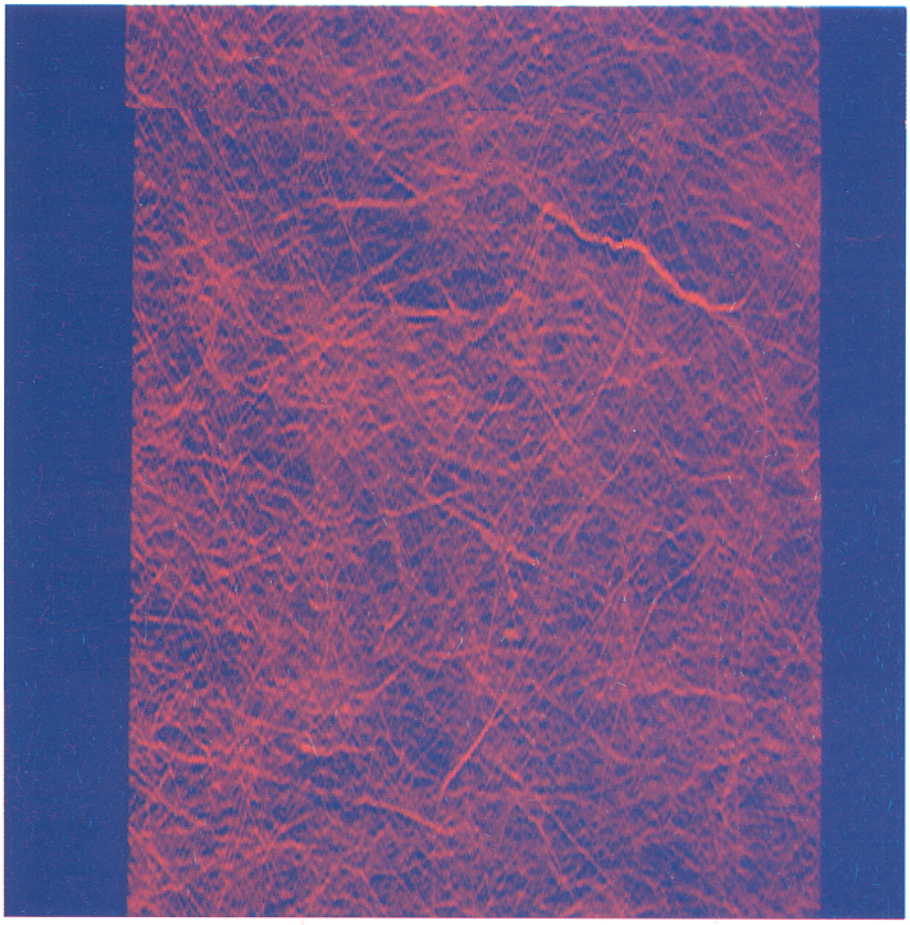

Fig. 9: Example 5

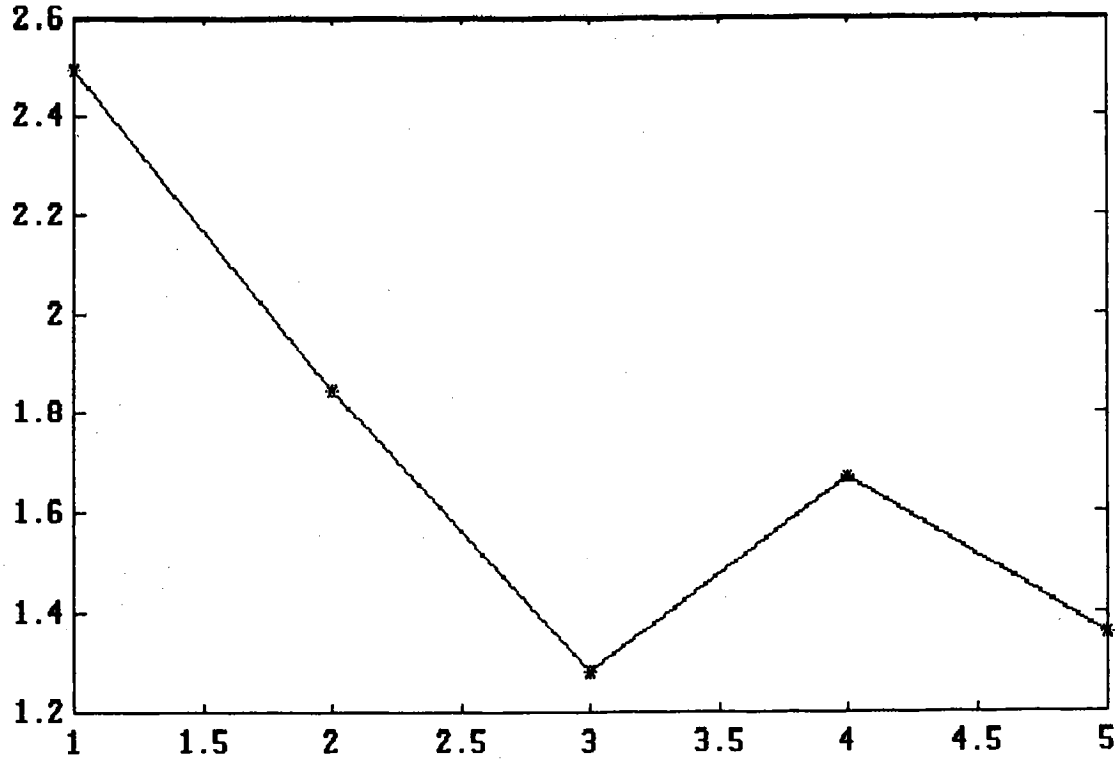

Fig. 10: $(\sigma^{jh})^2_{ex.3}$ / $(\sigma^{jh})^2_{ex.5}$ vs. j

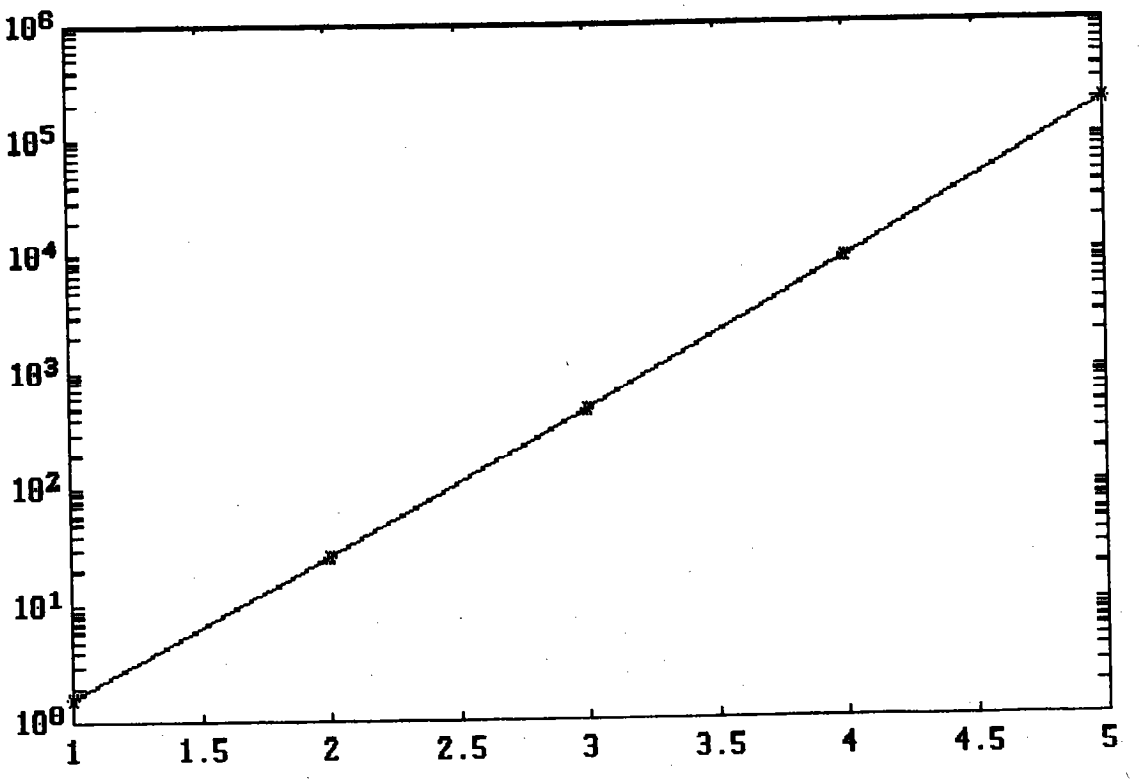

Fig. 11: Semilog plot of $(\tilde{\sigma}^{jh})^2_{ex.1}$ vs. j

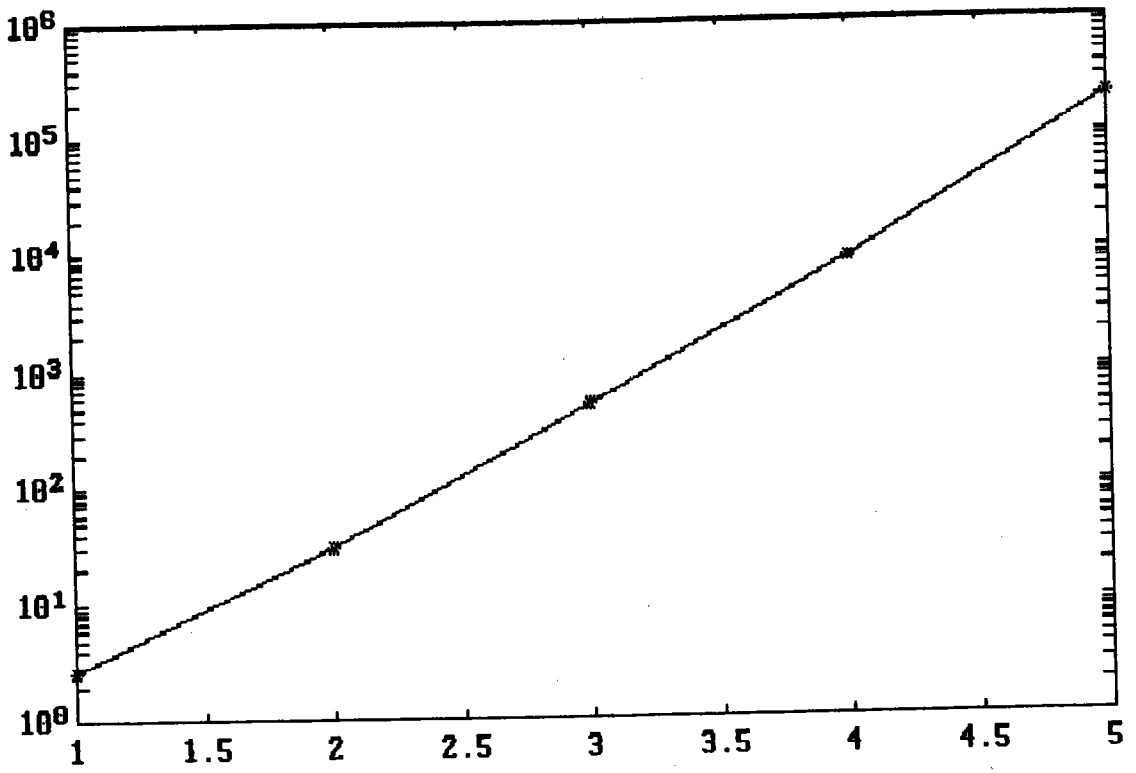

Fig. 12: Semilog plot of $(\tilde{\sigma}^{jv})^2_{ex.2}$ vs. j

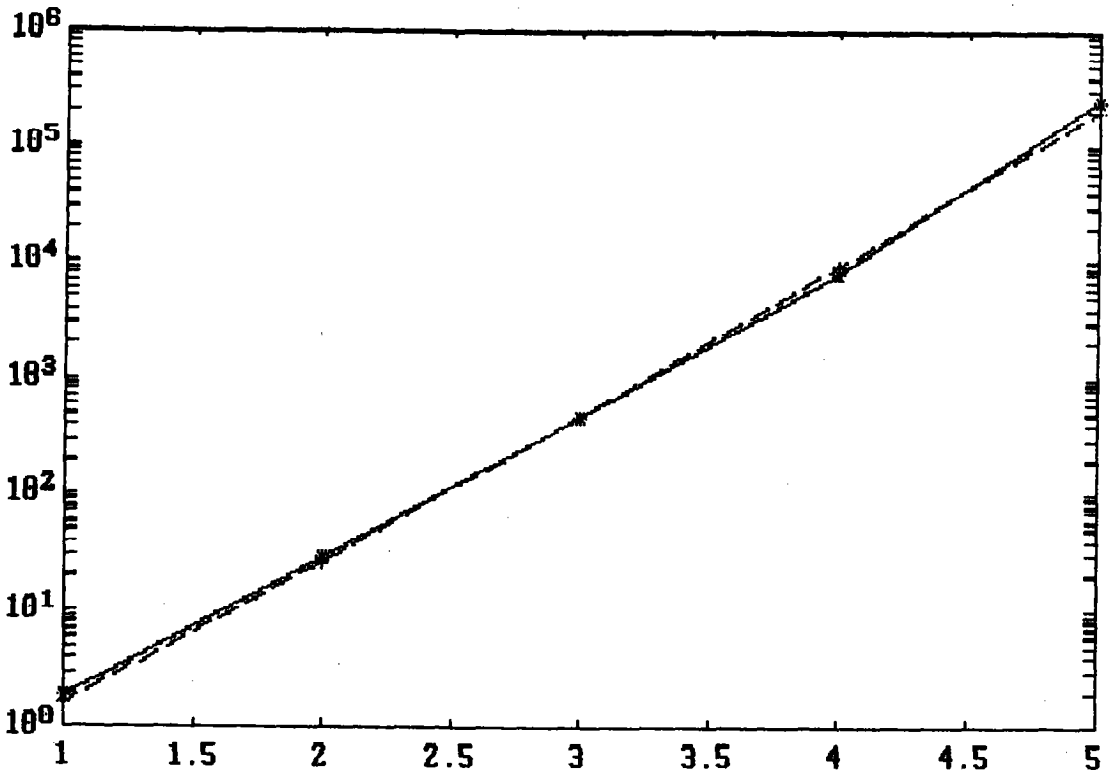

Fig. 13a: Semilog plot of $(\tilde{\sigma}^{jh})^2_{ex.4}$ (solid line) and $(\tilde{\sigma}^{jh})^2_{ex.1}$ (broken line) vs. j

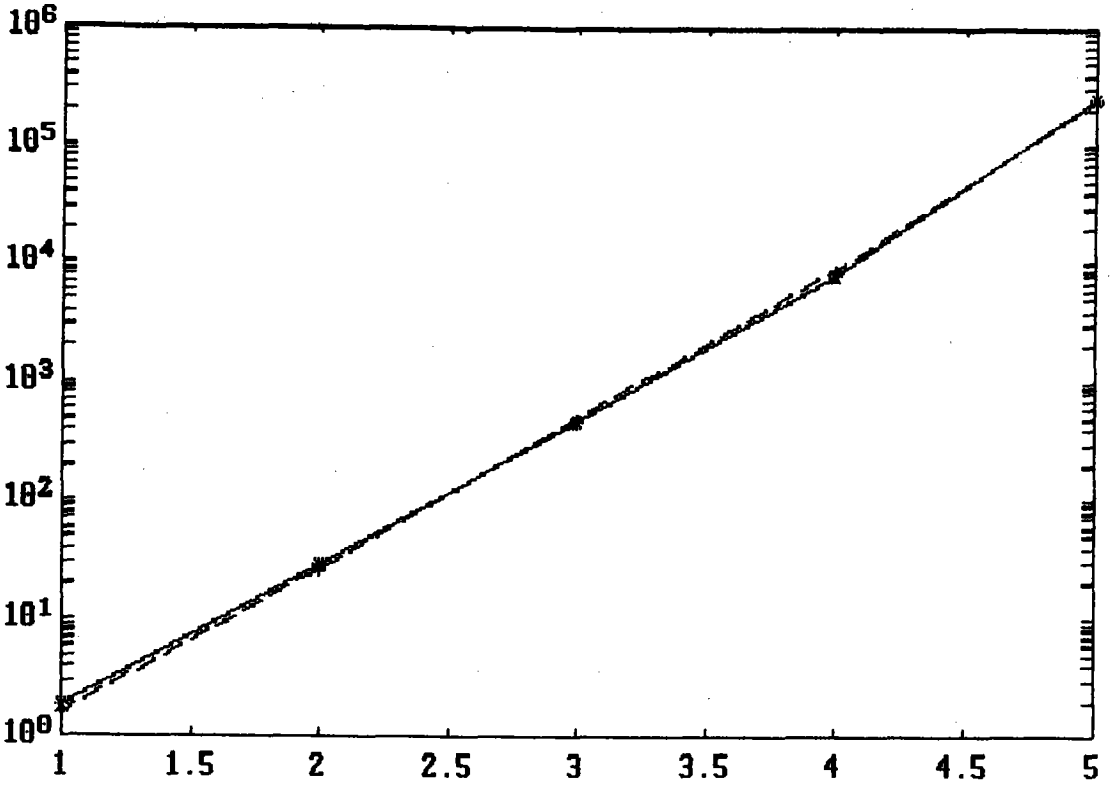

Fig. 13b: Semilog plot of $(\tilde{\sigma}^{jh})^2_{ex.4}$ (solid line) and $(\tilde{\sigma}^{jh})^2_{ex.2}$ (broken line) vs. j